Hindawi
Journal of Sensors
Volume 2018, Article ID 3675090, 9 pages
https://doi.org/10.1155/2018/3675090

Research Article

Metal Detection Sensor Utilizing Magneto-Impedance Magnetometer

Kyoo Nam Choi

Department of Information and Telecommunication Engineering, Incheon National University, Incheon 22012, Republic of Korea

Correspondence should be addressed to Kyoo Nam Choi; knchoi@inu.ac.kr

Received 23 February 2018; Revised 24 April 2018; Accepted 9 May 2018; Published 5 June 2018

Academic Editor: Lucio Pancheri

A magnetometer with a longitudinal sensing line using the MI effect was examined experimentally to find an application to replace conventional metal sensors based on an LVDT. A sampling to the second peak signal from the pickup coil on the sensing head with a long, thin soft magnetic ribbon and driven with an ultrashort pulse train with a pulse width of 5~7 ns formed the front end of the metal sensor. Unmatched degaussing and geomagnetic field compensation methods were effective not only to minimize the remnant magnetic field but also to prevent the saturation of the magnetic ribbon and expand the dynamic range. The active noise reduction process reduced the inherent noise to the 1/3 level with a minimum influence on the detection signal. The proposed metal sensor with unmatched degaussing, geomagnetic field compensation, and active noise reduction techniques demonstrated the detection of a 0.2 mm diameter magnetized ferrous ball.

1. Introduction

Metal detection sensors that use a linear variable differential transformer (LVDT) are widely used to detect foreign metal objects in food and in the security industry. This type of metal detector requires a strict balance between two differential inputs in various environmental conditions and complete shielding from external electromagnetic waves. Also, the sensitivity of detecting a foreign metallic object is influenced by the surrounding medium. It is hard for an LVDT-type sensor to detect a metallic object depending on placement angle. In the case of ferrous sphere, the detection resolution of an LVDT-type sensor is ~0.7 mm diameter [1]. The sensitivity of this metal sensor is dependent on the orientation of the metallic object, and it requires multiple sensors to detect ferromagnetic metal independent of object orientation [2]. A magnetometer is an alternative way to detect a magnetized metallic object inside an electric shield medium [3, 4]. A hall sensor is commonly used for magnetic field detection, because it has a simple structure; however, the sensitivity is not sufficient to detect a tiny magnetized metal object [5]. A magneto-resistance (MR) sensor has better resolution than a hall sensor [6], and a giant magneto-resistance (GMR) sensor has better resolution than an MR sensor [7]. Overall, the three sensors above have similar power consumption. Fluxgate [8], magneto-impedance (MI) [9], and giant magneto-impedance (GMI) [10] sensors have higher resolution in this magnetic sensor group. The fluxgate sensor has a lower internal noise level than MI or GMI sensors, but it consumes more power. Thus, a GMI sensor has the advantages of higher sensitivity, lower power consumption, and simple sensor head structure for metal detection applications, despite its relatively higher internal noise level. GMI sensors use a magneto-inductive effect at low frequency ranging from 1 to 10 kHz [11], skin effect at high frequency ranging from 10 kHz to 1 GHz [12], and a ferromagnetic resonance effect at ultrahigh frequency that is >1 GHz [13]. Among these, the GMI sensor that uses a skin effect has the advantage of low power consumption and high resolution. The sampling method [14] or the detection of higher harmonic frequency [15] has been attempted to reduce power consumption or increase sensitivity. A high-resolution micro-GMI sensor has been achieved using a pulse magneto-impedance effect inside a microamorphous wire [16]. This microsensor has shown pinpoint sensitivity at the sensor tip, but multiple sensors are required to cover the longitudinal sensing length. In

this paper, a method to enhance the sensitivity of a GMI sensor based on a single longitudinal amorphous ribbon is analyzed, and a method to reduce the noise component is investigated.

2. Design of MI Sensor Head

A magnetometer sensor element consists of a thin longitudinal amorphous ribbon and surrounding wound pickup coil. The impedance of a magnetic ribbon comes from the addition of DC resistance and inductive reactance that is determined by the skin effect. The DC resistance has a negligible effect, and the driving frequency and maximum differential permeability become the major determining factors for sensitivity. The magneto-inductive effect induces an inductive voltage across the pickup coil that is proportional to sqrt $(f\mu(H_{\text{ext}}))$, where f is the driving frequency, μ is the maximum differential permeability, and H_{ext} is the external magnetic field. In the case of pulse driving, the driving frequency corresponds to $1/2t_{\text{r}}$, where t_{r} is the pulse rising time. Also, a demagnetizing field prior to pulse excitation is necessary to prevent the accumulation of a magnetic field inside the core material. The magneto-impedance effect is measured by using the formula $\Delta Z/Z$, where Z is the impedance of the core material and ΔZ is the impedance difference when the external magnetic field is applied. However, in the case of driving with short pulses with a low duty cycle, the change of impedance due to an external magnetic field occurs only within a short duration that is proportional to the applied pulse width, which is in the ns range. Thus, the impedance variation due to the external magnetic field is captured at the instance when the short pulse is applied. And the captured signal response is for the real part of impedance variation due to the magneto-impedance effect. Thus, for sensor application, it is practical to directly measure the magneto-impedance effect as $\Delta V_{\text{o}}(H_{\text{ext}})/\min(V_{\text{o}})$, where $\min(V_{\text{o}})$ is the minimum output voltage at pickup coil, H_{ext} is the applied external magnetic field, and $\Delta V_{\text{o}}(H_{\text{ext}})$ is the output voltage difference when the external magnetic field, H_{ext}, is applied.

2.1. Sensor Head Structure. The sensor was intended to cover a longitudinal sensing length of 90 mm. A soft magnetic material was used as the sensor head core, as shown in Table 1. The pickup coil was wound on a bobbin surrounding the core, and the compensating coil was also wound on a circular bobbin surrounding the pickup coil to cancel the geomagnetic effect. The overall dimension of the core material, pickup, and compensating coils is shown in Tables 1 and 2. The shape of the sensing head is shown in Figure 1.

2.2. Sensitivity Distribution on a Sensor Head. The sensitivity of the sensor was tested along the sensing axis. The peak magnitude of a driving pulse with a width of 4.5 ns was fixed to 3.5 V. Output voltage variation in the first peak signal from the pickup coil responding to geomagnetic and external magnetic fields was measured, as shown in Figure 2. The total field strength of the geomagnetic field at the measurement location was 51 μT or 0.51 G (horizontal intensity of 29 μT, north component of 29 μT, east component of $-4\,\mu$T, and vertical component of 41 μT). The output voltage was derived by sampling and holding a peak value. The tip of the sensor head for positive driving pulse input was rotated along the earth's magnetic poles to evaluate influence by geomagnetic field. A rare earth pressed cube permanent magnet with dimensions of $L2 \times W2 \times H1$ mm and with 500 μT at a distance of 1 cm moved along the longitudinal direction of sensor head. When the tip of the sensor head for positive driving pulse input pointed to the north and the west, one end of the sensor head had the maximum sensitivity and gradually decreased toward the other end, as shown in Figure 2(a). This phenomenon was reversed when the tip of the sensor head for positive driving pulse input was reversed, as shown in Figure 2(b). When the tip of the sensor head for positive driving pulse input pointed to the northeast, both ends of the sensor head had sensitivity. This implies that the sensitivity of the sensor head is sufficient to be influenced by a geomagnetic field. Also, the sensor head has sensitivity not only at both tips but also on the side. The slightly distorted trend in Figure 2 is regarded to be due to a magnetic field from nearby electronic equipment.

2.3. Bipolar Driving. A soft magnet material in a core is magnetized in one direction if it is continuously driven by a unipolar pulse train, as shown in Figure 3(a). In the case of an MI sensor, this accumulates a magnetic field and results in either subtracting or adding to the magnetic field to be measured. One way to solve this erroneous result is by alternatively driving with a matched pulse pair with equal amplitude, but opposite polarity, as shown in Figure 3(b). This scheme is suited for degaussing purpose, but the response by one driving pulse is partially influenced by the other following degaussing pulse unless the two pulses are separated to a sufficient time interval within an acceptable influence level, because a degaussing pulse also induces an MI effect in the negative direction. The disadvantage of this scheme can be alleviated by programming with two different pulses, a driving pulse with a major MI effect and a degaussing pulse with a small MI effect, as shown in Figure 3(c). The physical adjustment is to set a driving pulse duration that induces a maximum MI effect and a degaussing pulse duration with more than 10 times the driving pulse duration. A driving pulse duration from 4.5 to 7 ns was tested to find the optimum pulse width for this experiment.

2.4. Reception Sensitivity. The core of the sensor head was driven by a positive polarity pulse with 4.5 ns width, t_{Drv}, with the degaussing pulse having opposite polarity from the width, t_{Deg}, as Figure 3(c). The peak magnitude of the driving pulse was measured as 3.5 V. The responding signal was measured from the signal pickup coil and had an oscillation waveform with more than 10 decaying peaks. Among them, the first four peaks had the significant responses against external magnetic field variation. A typical reception signal waveform is shown in Figure 4.

The same rare earth pressed magnet, with 500 μT at 1 cm distance, was moved to the center of the sensor head, and the variation of the reception signal waveform was measured, as shown in Figures 5(a) and 5(b). The waveform in channel 1

Table 1: Characteristics of core.

Layer	R	L	Dimension (mm)	Permeability	Material
1	4.1 Ω	4 μH	$L97 \times W1 \times T0.018$	$\mu_r = 5000$	VITROVAC 6205X (FeCo)SiB

Table 2: Characteristics of coil.

Coil type	Bobbin (mm)	Turns	Diameter	R	L
Signal pickup	$L87 \times W2 \times T3$	200	0.15 mm	3.1 Ω	247 μH
Compensating	$L18 \times D9$	100	0.15 mm	3.0 Ω	143 μH

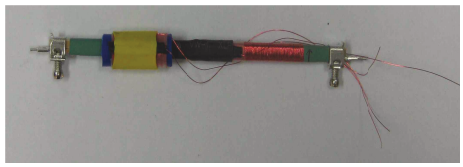

Figure 1: Shape of sensor head.

shows a reference pulse, and the waveform in channel 2 shows a signal waveform at the pickup coil. The reference pulse in Figure 5 indicates the starting point of the signal waveform from the pickup coil. Where a geomagnetic field was present and the tip of the sensor head for positive driving pulse input oriented to the west, the output voltage from the pickup coil was marked as a minimum output voltage, min (V_o), as shown in Figure 5(a). When an external magnetic field was approached, the output voltage from the pickup coil increased to a maximum output voltage, max (V_o), as shown in Figure 5(b). The effect on the real part of magneto-impedance was calculated as 600% for the first peak and 1180% for the second peak waveforms by using the formula in (1). This implies that the second peak has the biggest MI effect for a point magnetic field source in a longitudinal sensor geometry.

$$\frac{\Delta Z}{Z} = \frac{|\max(V_o) - \min(V_o)|}{|\min(V_o)|}. \quad (1)$$

Another experiment to investigate the effect of a uniform magnetic field such as a geomagnetic field was performed. The peak magnitude of driving pulse was fixed to 3.5 V, and the tip of the sensor head for positive driving pulse input was located to point the east and then rotated to point south. The output voltage variation in each peak signal waveform at the pickup coil was measured by varying the pulse width from 5 ns to 7 ns, as shown in Figure 6. The total magnetic field strength of the geomagnetic field at the measurement location was same as 51 μT or 0.51 G. The measurement results showed that the second peak had the biggest output signal variation, and the driving pulse with a 6.5 ns FWHM width had the greatest sensitivity. For the driving pulse of 6.5 ns FWHM, the effect of magneto-impedance was calculated as 2900% for the first peak and 1700% for the second peak waveforms. This indicates that the MI effect is the biggest for the first peak even though the variation of output signal voltage is the biggest for the second peak in a uniform geomagnetic field in a longitudinal sensor geometry.

The peak magnitude of the driving pulse was increased to 5.2 V for the purpose of investigating the effect of driving pulse amplitude, and the responding output signal showed a similar waveform, but with increasing amplitude. The same rare earth pressed magnet was moved to the center of the sensor head, and the output signal waveform was measured with and without an external magnetic field. The tip of the sensor head for positive driving pulse input was oriented to the west, and the output voltage was marked as minimum amplitude, min (V_o). A sample magnet was moved to a 10 mm distance from the center of the sensor head, and the output voltage was marked as maximum amplitude, max (V_o). The maximum output voltage, max (V_o), and a minimum output voltage, min (V_o), were compared, and the effect of magneto-impedance was calculated as 1160% for the first peak and 2100% for the second peak waveforms. This implies that the effect of magneto-impedance is almost proportional to the square of driving pulse voltage.

The output signal voltage at the pickup coil was monitored by continuously varying the driving pulse voltage to the soft magnet. The first peak output signal was found to be matched with the time at a peak of the driving pulse, and each peak value had a tendency to increase proportionally to a square of the driving pulse voltage, as shown in Figure 7. This implies that the output signal voltage is a function of driving pulse power.

The effect of driving pulse voltage on the MI index was measured by varying the driving pulse voltage to the soft magnet. The MI index had a tendency to increase proportionally to a square of the driving pulse voltage, as shown in Figure 8. Thus, the higher the driving voltage is, the better the magneto-impedance index is. However, an external magnetic field far beyond 500 μT at 1 cm distance resulted in the same or less output signal voltage due to saturation of the soft magnet.

Driving with a matched degaussing pulse, as shown in Figure 9(a), was compared with an unmatched degaussing pulse, as shown in Figure 9(b), in a constant geomagnetic field. The driving pulse width was set to 5 ns, and the product of pulse width and pulse magnitude between driving and degaussing pulses was kept equal. The measurement results, as shown in Figure 10, showed that the response of the first peak signal was bigger than the response of the second peak signal in the case of matched degaussing. On the contrary,

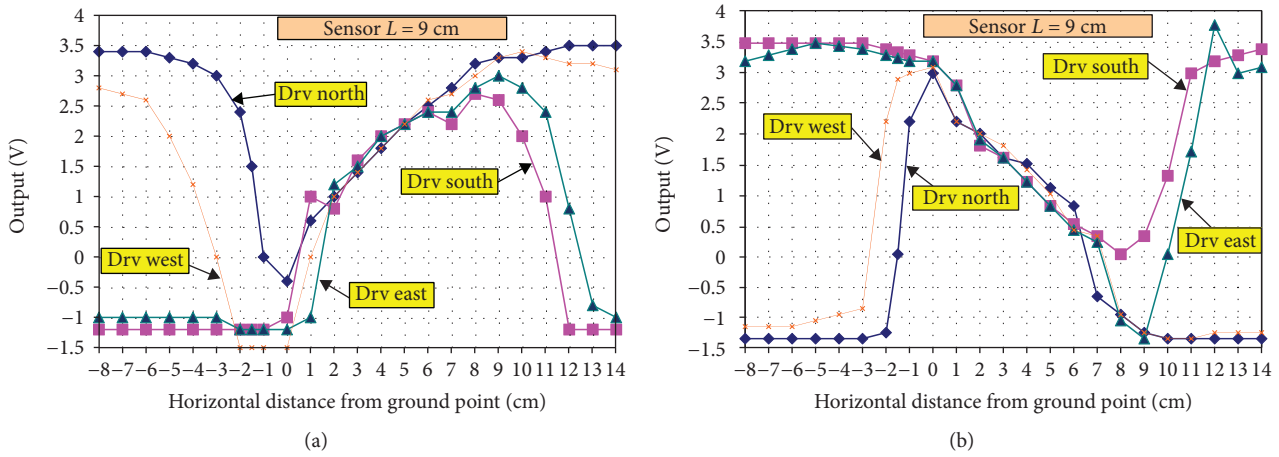

Figure 2: Sensitivity of the sensor head along longitudinal direction. (a) Forward driving. (b) Reverse driving.

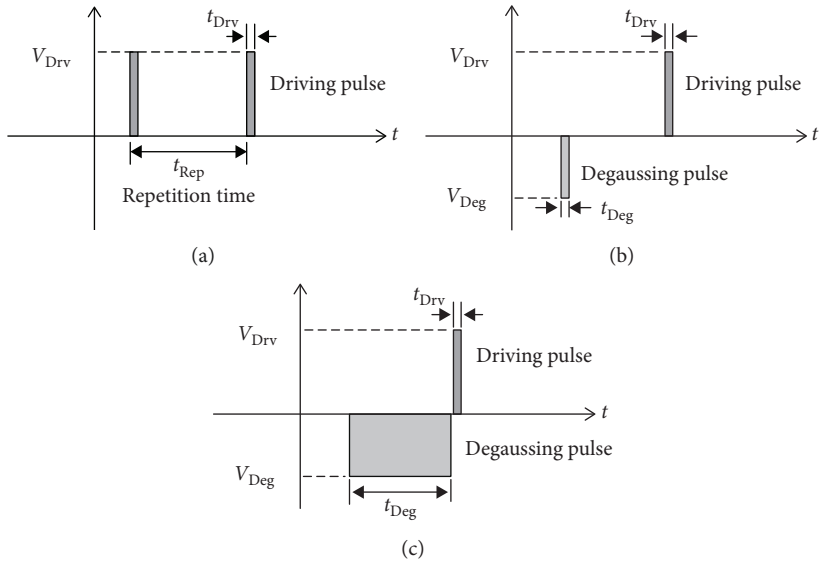

Figure 3: Driving pulse waveform of soft magnet with driving amplitude V_{Drv} and degaussing amplitude V_{Deg}. (a) Unipolar driving. (b) Driving with matched degaussing. (c) Driving with unmatched degaussing.

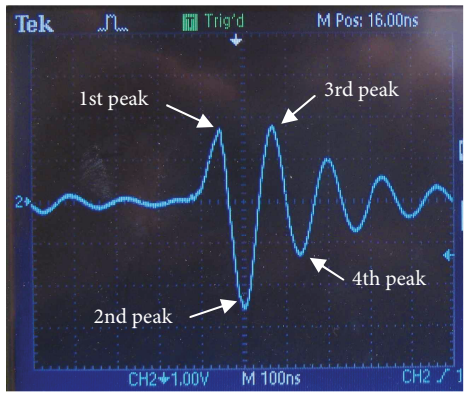

Figure 4: Signal waveforms at the pickup coil when driving with a pulse amplitude of 3.5 V.

the second peak signal was bigger than the first peak signal in the case of unmatched degaussing. The dynamic range of the output signal was found to be bigger in the case of unmatched degaussing for both first and second peak signals. This indicates that driving with an unmatched degaussing pulse induces a bigger response against external magnetic field variation.

The effect changing the number of soft magnet layers was investigated using the same sensor head structure. The driving pulse voltage was kept at 3.5 V, and the driving pulse width was set to 5 ns FWHM in a uniform geomagnetic field. An unmatched degaussing pulse was followed by a driving pulse for comparison under the same experiment conditions. The output swing range was reduced to half in the case of two layers for the first peak signal. For the second peak signal, this reduction rate was decreased to one-third in comparison to one layer of soft magnet, as shown in Figure 11(a). In the

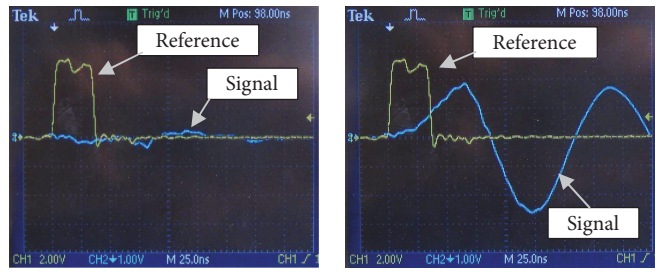

(a) (b)

Figure 5: Signal waveforms at the pickup coil when driving with 3.5 V pulse amplitude. (a) Without external magnetic field. (b) With external magnetic field.

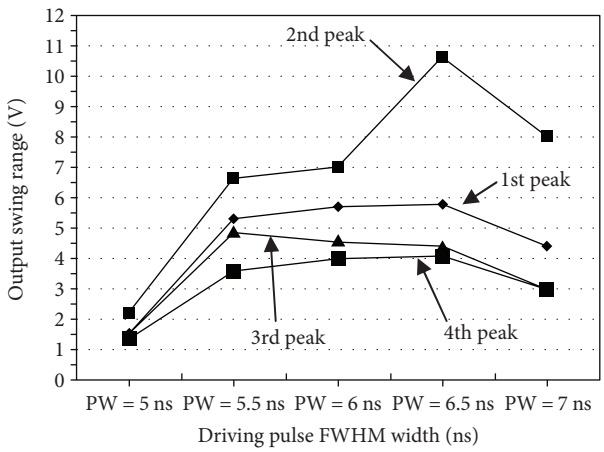

Figure 6: Variation of output signal voltage responding to uniform geomagnetic field when driving with 3.5 V pulse amplitude.

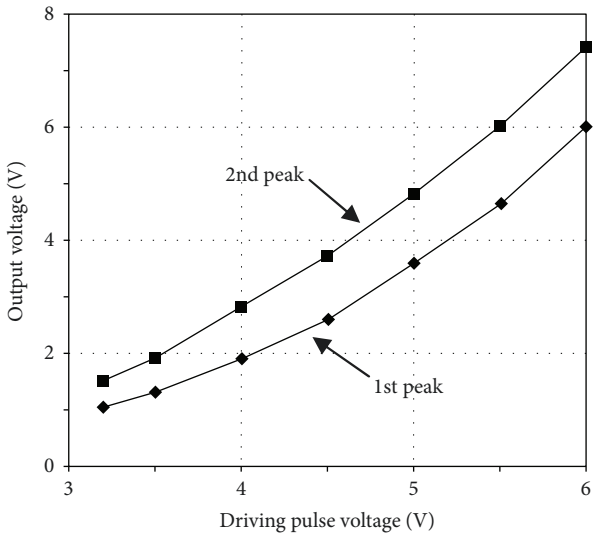

Figure 7: Signal output voltage at the pickup coil as a function of driving pulse voltage.

following experiment, the driving pulse voltage was increased to 5.2 V, and a sample magnet was moved to a 10 mm distance from the center of the sensor head. With this experiment setup, the effect on the MI index was investigated by

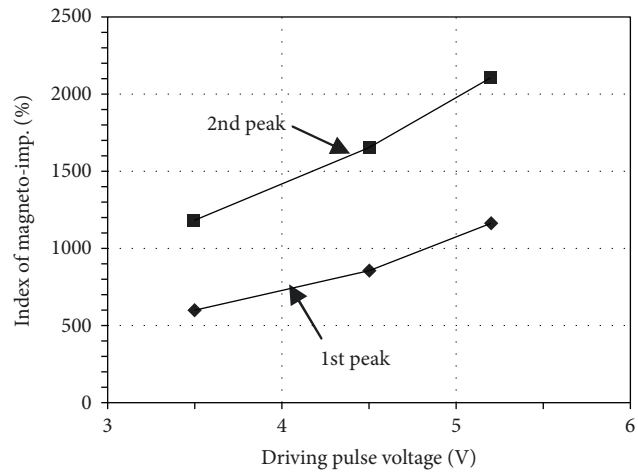

Figure 8: Magneto-impedance index of output signal at the pickup coil as a function of driving pulse voltage.

changing the number of soft magnet layers. The MI index was reduced to 30% in the case of two layers for the first peak signal. For the second peak signal, this index reduction was cut to one-tenth in comparison to one layer of soft magnet, as shown in Figure 11(b). This indicates that increasing the number of soft magnet layers results in reduced sensitivity.

3. Metal Detection Sensor

3.1. Metal Sensor Circuit. A metal detection sensor using a magneto-impedance effect was fabricated. The soft magnetic strip of the sensor head was driven through the soft magnet driver by using a pulse train generator, which is composed of a driving pulse and unmatched degaussing pulse. The soft magnet driver is an electronic amplifier that supplies more current to the soft magnet with low impedance by means of impedance matching. The pulse widths were 6.5 ns and 60 ns, respectively. The effect due to geomagnetic field was canceled by adding a null current to the compensating coil of the sensor head. The sampling signal was delayed to sample the desired peak amplitude from the pickup coil by using a variable delay circuit. A driver circuit block diagram of the soft magnetic strip is shown in Figure 12. The reception signal was sampled and held to effectively recover the variation of second peak amplitude from the pickup coil. The product of pulse

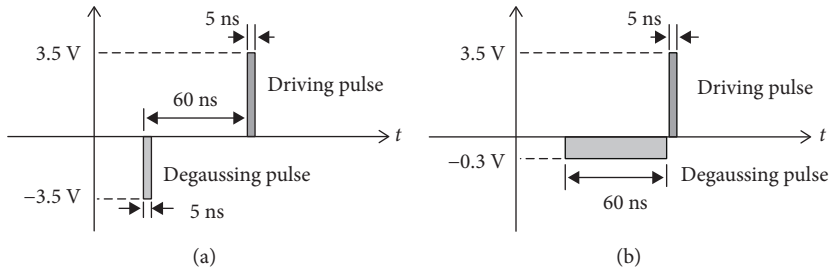

Figure 9: Driving pulse waveform of soft magnet with 5 ns width and degaussing pulse waveform. (a) Driving with matched degaussing. (b) Driving with unmatched degaussing.

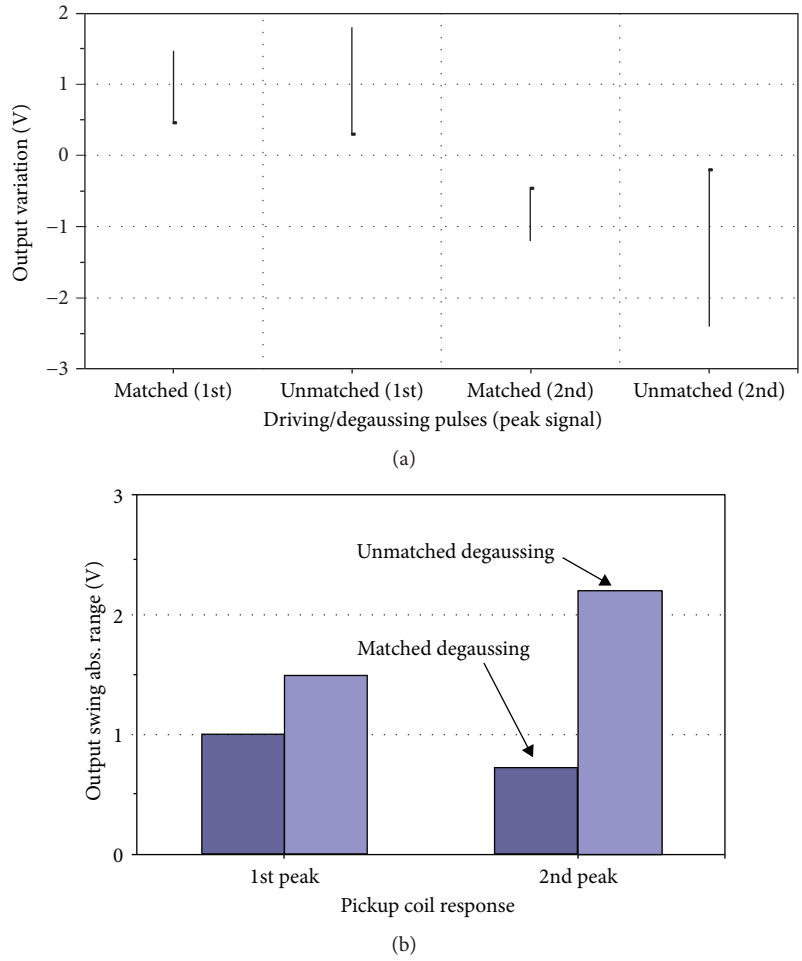

Figure 10: Comparison of output signal voltage between matched and unmatched degaussing, responding to geomagnetic field when driving with 3.5 V pulse amplitude. (a) Signal voltage variation. (b) Absolute value of signal voltage variation.

amplitude by pulse width between the driving pulse and the degaussing pulse was kept equal. The feedback signal from the receiver was used to minimize the effect by residual magnetic field by adjusting the amplitude of the degaussing pulse.

A high impedance buffer was used to preserve the waveform from the pickup coil, and a low leakage capacitor was used to hold the sampling signal. The DC level of the sample-and-hold signal was measured and converted to drive a compensation coil for the purpose of geomagnetic field cancelling. The external noise component was attenuated by using an 8th order Bessel passive noise filter with a variable cutoff frequency. Amplification followed, typically 20,000 times, but with a variable range of 40~50,000 times. The residual noise component, which was inherent in the MI sensor, was reduced by using an active noise filter. Finally, the presence of metal was determined by adjusting the threshold level in the detection circuit. A block diagram of the receiver part is shown in Figure 13.

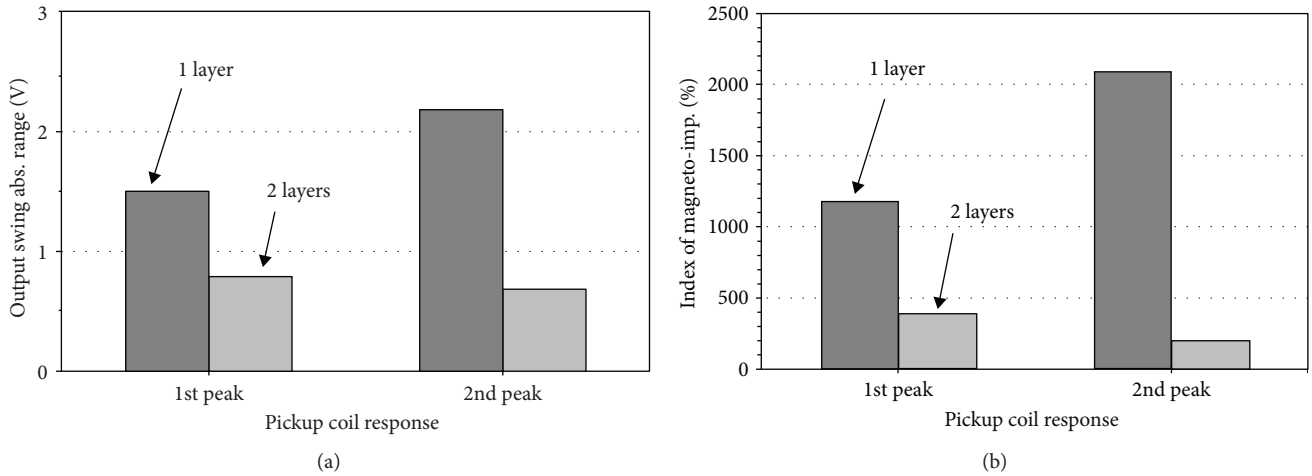

Figure 11: Comparison of output signal voltage between one and two soft magnet layers when driving with 5 ns pulse width. (a) Output voltage swing range. (b) MI index.

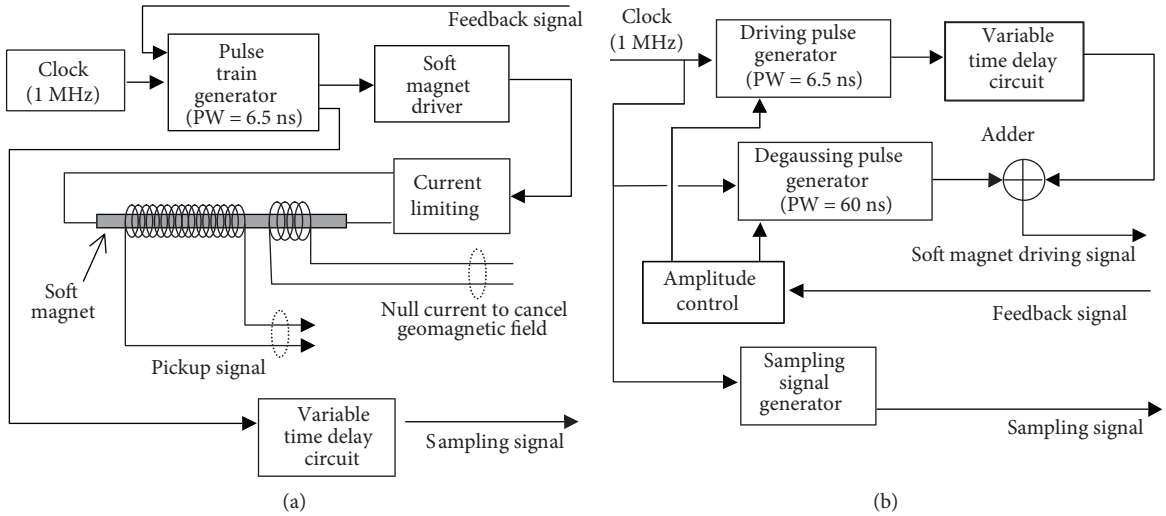

Figure 12: Sensor head driver circuit. (a) Block diagram of soft magnet driver. (b) Block diagram of pulse train generator.

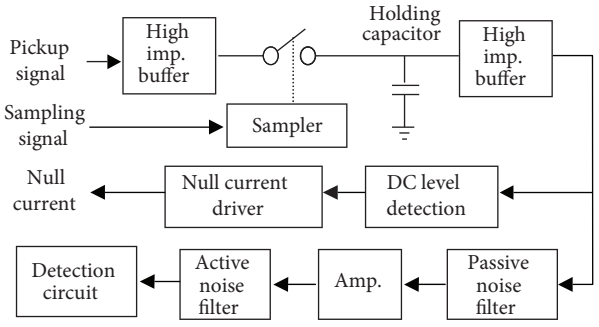

Figure 13: Block diagram of receiver circuit.

3.2. Active Noise Reduction. The reception signal from the MI sensor head contains irregular background noise with a wide frequency spectrum, which is hard to reduce by using a conventional passive filter. The characteristic of this noise is not a simple Fourier series frequency component but a mixture of multiple frequency and phase reversal components. Also, if we decrease the threshold point low enough to detect tiny metal objects at micron scale, the magnitude of noise contains a burst component that can be greater than the detection signal and lies in a higher frequency band. The movement of metal objects to be detected is within a lower frequency band of background noise, but it is slower than the period of mixed frequencies. If a metal object triggers an amplitude signal that is bigger than the noise level but wider in time period, the detection signal contains a big wave in a lower frequency band and small noise waves with mixed frequency. The active noise reduction (ANR) method cancels the noise signal with mixed frequency and even bigger burst component, but recovers a detection signal in a lower frequency band and even smaller amplitude than a noise burst. A diagram showing the ANR methodology is shown in Figure 14(a), and a controller in Figure 14(b). Inside the controller, a slow-varying component is removed, and a fast-varying component is recovered by using a differentiator.

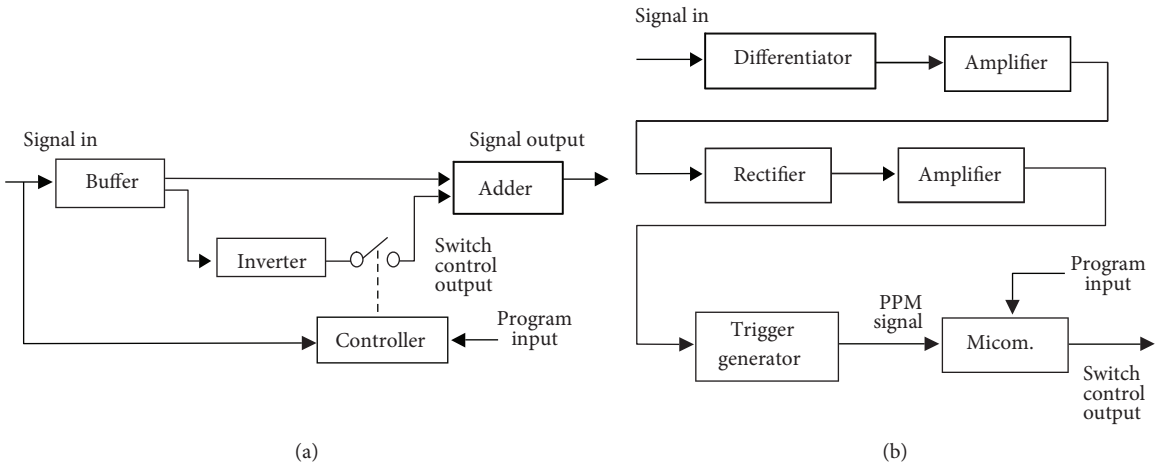

Figure 14: Method of active noise reduction. (a) Block diagram of ANR. (b) Controller of ANR.

This method is effective in removing low-frequency components in noise with a mixed frequency, while a detection signal with a longer time interval is also filtered out by using a conventional filter. After amplification and rectification followed by a trigger generator, it is converted to a pulse position modulation (PPM) signal. By using this PPM signal, a microprocessor determines the presence of a metal object by counting the pulse interval. An example showing the effect by active noise reduction is shown in Figure 15.

3.3. Metal Detection. The metal detection sensor with a longitudinal sensor geometry has a varying DC response depending on the longitudinal position at the sensor head and the angle of the sensor head with a geomagnetic field axis. However, an AC small signal response has sensitivity independent of the longitudinal position at the sensor head and the position angle with a geomagnetic field axis, because it senses a difference in signal variation. The DC response was kept to a null point by flowing a current in a compensation coil; thus, it prevented saturation in the soft magnet and enabled a dynamic range expansion. An AC small signal response can be amplified within the margin of the signal-to-noise ratio (SNR), and the ANR method can be applied to increase this SNR. The detection signal responding to a 0.2 mm diameter magnetized ferrous ball is shown in Figure 16. The first peak represents the presence of the magnetized metallic object, and the second small peak is due to unfiltered noise after ANR, which limits the minimum resolution of this magnetometer. The captured analog signal waveform before digital signal processing showed a discernible response to a magnetized metal object.

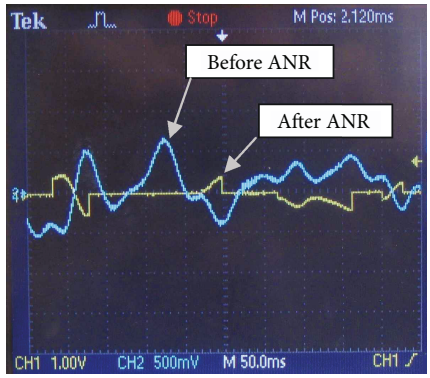

Figure 15: Noise waveform. CH1: after ANR; CH2: before ANR.

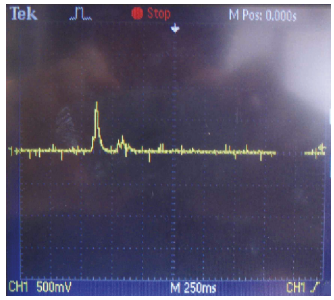

Figure 16: Metal detection waveform responding to 0.2 mm diameter ferrous ball.

4. Conclusion

A magnetometer with a longitudinal sensing line using the MI effect was examined experimentally to find an application to replace conventional metal sensors based on an LVDT. The sensing head consisted of a thin, 90 mm ribbon and surrounding wound pickup coil and was driven with an ultrashort pulse train with a pulse width of 5~7 ns. The unmatched degaussing methods were used to minimize the remnant magnetic field, and a compensation coil in the sensor head prevented the saturation of the sensor head and contributed to expand the dynamic range to external magnetic field variation. A noise reduction process using an ANR algorithm was effective in removing noise with mixed frequency components without influencing the detection signal with a longer time interval. A magnetized ferrous ball was used to examine the metal detection capability. The metal sensor in this experiment showed discernible responses to detect a 0.2 mm diameter magnetized metal object.

Data Availability

The data used to support the findings of this study are available from the corresponding author upon request.

Conflicts of Interest

The author declares that there is no conflict of interests regarding the publication of this paper.

Acknowledgments

This work was supported by Incheon National University Research Grant in 2017.

References

[1] K. N. Choi, "Characteristics of metal sensor using variable frequency," *The Journal of the Korea Institute of Electronic Communication Sciences*, vol. 9, no. 2, pp. 161–166, 2014.

[2] K. N. Choi, "Two-channel metal detector using two perpendicular antennas," *Journal of Sensors*, vol. 2014, Article ID 412621, 11 pages, 2014.

[3] E. Arribas, I. Escobar, C. P. Suarez, A. Najera, and A. Beléndez, "Measurement of the magnetic field of small magnets with a smartphone: a very economical laboratory practice for introductory physics courses," *European Journal of Physics*, vol. 36, no. 6, article 065002, 2015.

[4] A. Bergen, H. J. van Weers, C. Bruineman et al., "Design and validation of a large-format transition edge sensor array magnetic shielding system for space application," *Review of Scientific Instruments*, vol. 87, no. 10, article 105109, 2016.

[5] M. Zhelamskij, "The active magnetic tracking with scalable coverage: indoor navigation for smartphones," *Journal of Sensors and Sensor Systems*, vol. 5, no. 2, pp. 355–371, 2016.

[6] T.-H. Tran, P. Chao, and P.-C. Chien, "The front-end readout as an encoder IC for magneto-resistive linear scale sensors," *Sensors*, vol. 16, no. 9, article 1416, 2016.

[7] M. Sakthivel, B. George, and M. Sivaprakasam, "A novel GMR-based eddy current sensing probe with extended sensing range," *IEEE Transactions on Magnetics*, vol. 52, no. 4, pp. 1–12, 2016.

[8] M. F. Snoeij, V. Schaffer, S. Udayashankar, and M. V. Ivanov, "Integrated fluxgate magnetometer for use in isolated current sensing," *IEEE Journal of Solid-State Circuits*, vol. 51, no. 7, pp. 1684–1694, 2016.

[9] T. Wang, Y. Zhou, C. Lei et al., "The disturbing effect of the stray magnetic fields on magnetoimpedance sensors," *Sensors*, vol. 16, no. 10, article 1723, 2016.

[10] A. Talaat, M. Churyukanova, J. M. Blanco, M. Ipatov, V. Zhukova, and A. Zhukov, "Simultaneous detection of giant magnetoimpedance and fast domain wall propagation in Co-based glass-coated microwires," *IEEE Magnetics Letters*, vol. 7, pp. 1–4, 2016.

[11] E. M. Kardoulaki, R. R. A. Syms, I. R. Young, and M. Rea, "SNR in MI catheter receivers for MRI," *IEEE Sensors Journal*, vol. 16, no. 6, pp. 1700–1707, 2016.

[12] S. Y. Liu, Q. P. Cao, X. D. Wang et al., "Effects of thickness on structure and magnetic property of Fe-Y-B thin films," *Thin Solid Films*, vol. 616, pp. 608–617, 2016.

[13] K. Lenz, E. Kosubek, K. Baberschke et al., "Magnetic properties of Fe_3Si/GaAs(001) hybrid structures," *Physical Review B*, vol. 72, no. 14, 2005.

[14] S. Tajima, Y. Okuda, T. Watanabe, H. Aoyama, M. Yamamoto, and T. Uchiyama, "High-resolution magneto-impedance sensor with TAD for low noise signal processing," *IEEE Transactions on Magnetics*, vol. 50, no. 11, pp. 1–4, 2014.

[15] J. J. Beato-López, J. I. Pérez-Landazábal, and C. Gómez-Polo, "Magnetic nanoparticle detection method employing nonlinear magnetoimpedance effects," *Journal of Applied Physics*, vol. 121, no. 16, article 163901, 2017.

[16] S. Sandacci, D. Makhnovskiy, L. Panina, K. Mohri, and Y. Honkura, "Off-diagonal impedance in amorphous wires and its application to linear magnetic sensors," *IEEE Transactions on Magnetics*, vol. 40, no. 6, pp. 3505–3511, 2004.